European Review for Medical and Pharmacological Sciences 2015; 19: 256-264

Magnetic resonance venography in the diagnosis of inferior vena cava obstruction in Budd-Chiari syndrome

X. LU[1], C. YANG[1], K. XU[1], Y.-T. RONG[1], S.-D. LI[1], J.-S. LI[1], C.-F. HU[1], Q. SONG[1], P. MA[2], Q.-Q. ZHANG[3], H. XU[3], M.-H. ZU[3]

[1]Department of Radiology, [2]Clinical Laboratory, [3]Department of Interventional Radiology, The Affiliated Hospital of Xuzhou Medical College, Xuzhou, China

Xin Lu and *Chun Yang* contributed equally to this work and should be considered co-first authors

Abstract. – OBJECTIVE: To evaluate the informativeness of magnetic resonance venography (MRV) in the diagnosis of different types of inferior vena cava (IVC) obstruction.

PATIENTS AND METHODS: 56 patients with IVC obstruction underwent MRV scans. These scans were evaluated for morphology of the obstruction and compared with digital subtraction angiography (DSA) images.

RESULTS: Using DSA, we determined that 47 patients had complete obstruction and 9 had partial obstruction. MRV scans revealed 6 cases of partial obstruction. Using MRV, we determined the morphology of the proximal and distal ends of the complete obstructions in the IVC. We classified our observations into cone, plateau, and irregular subtypes. Both DSA and MRV scans were compared to assess the consistency between two methods. MRV demonstrated high sensitivity (100%) for diagnosing a complete obstruction of the IVC, and its specificity was 66.7%. The positive and negative predictive values of MRV were 94% and 100%, respectively.

CONCLUSIONS: MRV imaging is a valuable alternative to DSA for detection of obstructions in the IVC in Budd-Chiari syndrome, particularly in the distal end, which could expedite the decision making for interventional treatment programmes. However, MRV imaging is less suitable for observing the morphology of the proximal ends of obstructions due to the limitations of the scanning plane and the influence of pseudo shadows.

Key Words:
Vena cava inferior, Magnetic resonance venography, Vena cava occlusion.

Introduction

Intravascular interventional techniques used to treat Budd-Chiari Syndrome (BCS) have been well documented[1-7]. The success of interventional treatment and the appearance of complications are closely related to the anatomy of the occluded site in the inferior vena cava or the hepatic vein[8-10]. Magnetic resonance venography (MRV) has several advantages over digita subtraction angiography (DSA) for the diagnosis and classification of BCS[11-15]. Thus, MRV is less invasive. Further, it does not require injection of iodinated contrast solution and, therefore, limits the risk of allergic reactions. In addition, MRV does not expose the patient to radiation. MRV provides excellent resolution in soft tissue imaging and reflects pathological changes in the obstruction in an accurate and detailed manner. One MRV scan simultaneously assesses both the proximal and distal ends. Also, MRV imaging scans the obstruction in the inferior vena cava at multiple angles, thereby, providing information supplemental to DSA imaging. Moreover, MRV imaging substantially prolongs the time-to-treatment window established by computed tomographic venography (CTV). Additionally, due to the difference in the degree and scope of the obstruction, the peak of angiographic contrast agents may differ in BCS patients, which adds another obstacle to DSA. MRV overcomes these limitations, provides more explicit and reliable images of vein lesions, and has a higher rate of successful scans. However, the use of MRV for detecting the morphology of the occluded inferior vena cava is rarely reported. In this study, we compared MRV imaging of inferior vena cava obstructions with DSA imaging, and evaluated the usefulness of MRV in clinical settings.

Corresponding Author: Kai Xu, Ph.D; e-mail: xkpaper@163.com

Patients and Methods

Patient Information

Fifty-six patients with IVC occlusions (34 male and 22 female patients; age ranging from 19 to 78 years; mean [±SEM] age of 46 ± 8 years), who were treated in our Hospital between January 2010 and June 2011, were included in this study. The disease duration in these patients ranged from 3 months to 20 years, manifesting clinically as abdominal distension and pain, hepatosplenomegaly, abdominal and lower extremity varicosity, ascites, lower extremity edema, hyperpigmentation and ulcers. All patients underwent both MRV and DSA exams within 1 week, and then underwent interventional treatments. The procedures described below were carried out in accordance with the ethical standards of the Xuzhou Medical College Hospital Ethics Committee.

MRV Exam

A GE Sigma Excite 3.0 Tesla MRI whole body imaging system (GE Healthcare, Milwaukee, WI, USA) equipped with an 8 channel phase array abdomen TORSOPA coil was used. Conventional T1W1/T2W1 and FIESTA sequences were used to collect data. The MRV scan parameters consisted of a breath-hold fast liver accelerated volume acquisition (LAVA) volume scanning sequence in 3D mode using a 288×256 matrix, a 12° flip angle, 83.33 Hz bandwidth, a 40 cm field-of-view (FOV), and a 4.4 mm thickness. The forearm venous catheter was connected to a high-pressure injector (Ulrich, Ulm, Germany), and the enhanced contrast agent used was gadolinium-DTPA (0.1 mmol/kg, Bayer Schering Pharma AG, Guangzhou, China). After injection of enhanced contrast agent, 20 ml of saline were used to flush the circulation. The reconstruction of the MRV scan was based on the maximum intensity projection (MIP) of the original images. Virtual endoscopy using the coronal position as the standard position was employed to observe the anatomy of the IVC obstruction.

DSA Exam

A GE Innova-4100 flat-panel digital subtraction angiographic imaging system (GE Healthcare, Milwaukee, WI, USA) was used to collect the data. A 5F pigtail catheter was delivered to the lower edge of the occluded IVC via the femoral vein and 25-35 ml of Iobitridol (300 mg I/ml; Guerbet, Roissy, France) was injected at a flow rate of 15 ml/sec. Posterior-anterior position DSA was performed. Patients who presented with a complete IVC occlusion by one-way angiography underwent two-way angiography by jugular vein cannulation using a 5F single curve catheter. Patients, whose partial IVC occlusion was detected by one-way angiography, did not undergo two-way angiography.

Image Analysis

MRV images were read and scored as completely or partially occlusion by two expert radiologists. When inconsistent evaluations came out, consultation was used to reach a consensus on them. The DSA and MRV images of complete obstructions in the inferior vena cava were classified into cone, plateau and irregularly-shaped. A complicated thrombosis or the existence of collateral vessels was observed in all 56 cases of BCS.

Statistical Analysis

The scored MRV images were compared to scored DSA images for consistency using a paired chi-square test, and the value was calculated with $p < 0.01$ being set as statistically significant.

Results

The degree of IVC Obstruction

Of the 56 total BCS patients, 47 showed complete IVC occlusion and 9 showed partial IVC occlusions, as visualized using DSA imaging. Among 9 patients with partial IVC occlusion, 6 cases were partially obstructed in the membrane and 3 cases had segmental stenosis. Two out of the 47 patients with complete IVC occlusions had dangerous collateral vessels (one or several abnormally-running vessels originating from the obstructed side of the IVC), or locally distorted and expanded vessels. When MRV was performed, it correctly diagnosed the existence of an occlusion, but it did not permit visualization of the lumen in the stenotic segment in 2 patients. Thus, these 2 cases were incorrectly diagnosed as complete occlusion. In contrast, DSA enabled the visualization of contrast in the stenotic segments. MRV also resulted in the misdiagnosis of one case with partial occlusion that presented with a membranous obstruction combined with thrombosis (Table I).

Table I. Comparison of 56 cases of IVC obstruction diagnosed using MRV and DSA.

MRV			DSA							Total
			Complete blockage					Partial blockage		
			Proximal end		Distal end			Stenotic segment	Membrane with holes	
			Cone	Plateau	Cone	Plateau	Irregular			
Complete blockage	Proximal end	Cone	44				2	1	50	
		Plateau		3						50
	Distal end	Cone			37			2	1	
		Plateau				5				
		Irregular					5			6
Partial blockage		Stenotic segment						1		
		Membrane with holes							5	
	Total		47			47		9		56

MRI measurements of the holes in the membranous obstructions that were observed in some patients ranged from 2.6 to 9 mm. A "jet sign" could be observed in all patients of this type (Figures 1 and 2). Due to the variable size of the holes, the jet sign presented as a stripe of varying width like a flow void signal.

The Morphology of the Occluded end Proximal to the Heart

The morphology of complete obstructions in 47 patients included cone-shaped and plateau-shaped obstructions on the side proximal to the heart (Figures 3 and 4). The cone-shaped occlusions were observed in 44 cases and plateau-shaped occlusions were present in 3 cases. MRV led to misdiagnosis of 1 plateau-shaped occlusion as cone-shaped. The consistency rate between MRV and DSA was 95.7% in the diagnosing the morphology of occlusion on the side proximal to the heart.

The Morphology of the Occluded End Distal to the Heart

The morphologies of complete obstructions in 47 patients were cone-shaped (Figure 4), plateau-shaped (Figures 5 and 6) and irregularly-shaped (Figures 7 and 8) on the side distal to the heart.

Figure 1. MRV image of membranous obstruction in the IVC. The membrane was not clear, but jet sign is visible (*arrow*).

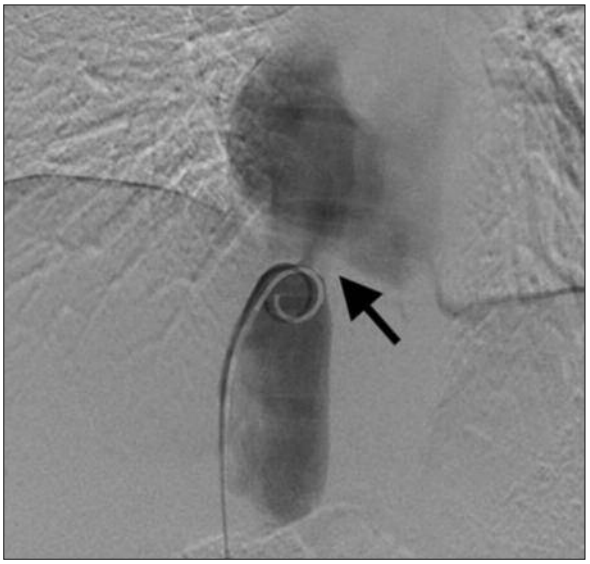

Figure 2. DSA image of membranous obstruction in the IVC. The jet sign is indicated by an arrow.

The cone-shaped occlusions were observed in 37 cases; 2 out 37 cases were combined with dangerous collateral vessels (Figures 9 and 10). The irregularly-shaped occlusions were observed in 5 cases, while platform-shaped occlusions were seen in 5 cases. MRV correctly diagnosed the morphology of the occluded end distal to the heart when the cases were combined with thrombosis, as the morphology was predominantly membranous in nature. Therefore, the consistency rate of MRV and DSA was 100% for diagnosing the morphology of the occluded end distal to the heart.

The IVC-associated Collateral Vessels and Thrombosis

DSA detected 25 cases with multiple collateral vessels on the distal side of the IVC (Figure 8), 2 cases with cone-shaped occlusions with collateral vessels, and 1 case with segment stenosis com-

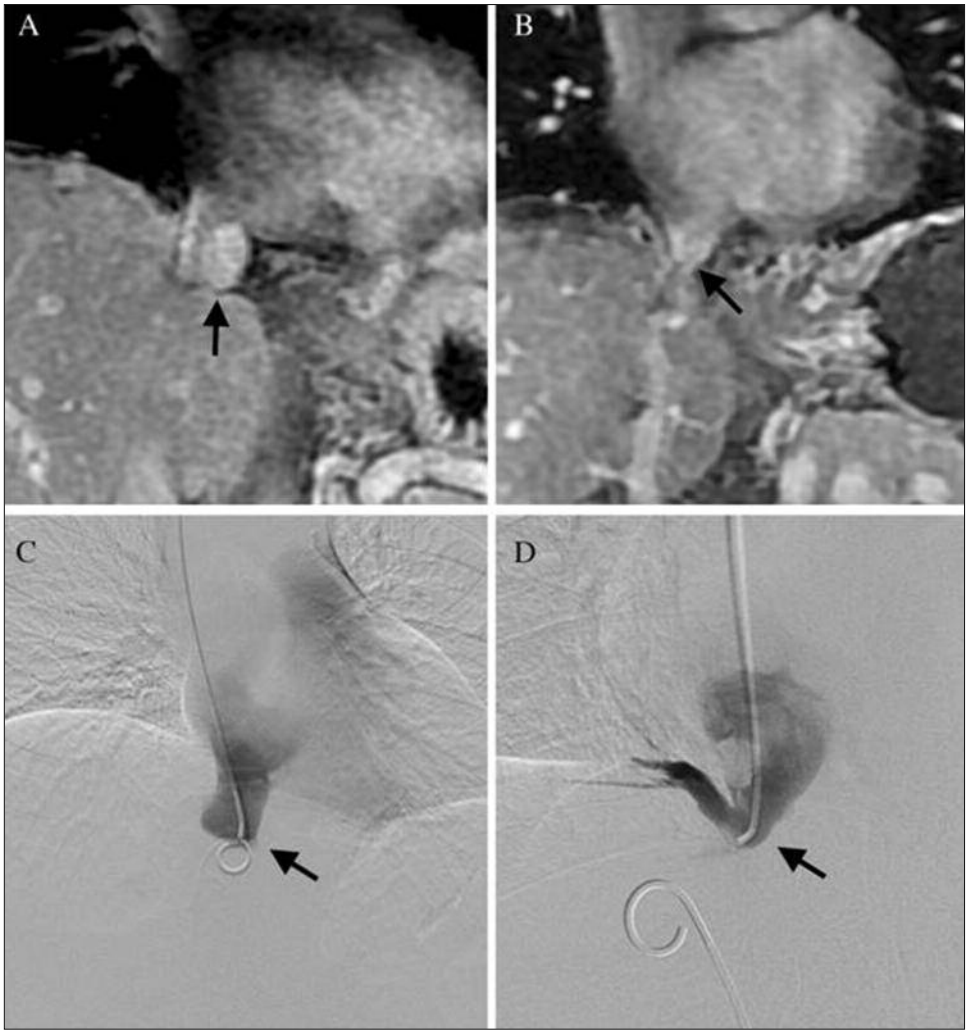

Figure 3 ***B,*** MRV and DSA images of the morphology of the proximal ends of IVC obstructions. ***A,*** and ***B,*** MRV images. ***C,*** and ***D,*** DSA images. ***A,*** A platform-shaped end is shown (arrow). ***B,*** A cone-shaped end is shown (*arrow*). ***C,*** A platform-shaped end is shown (*arrow*). ***D,*** A cone-shaped end is shown (*arrow*).

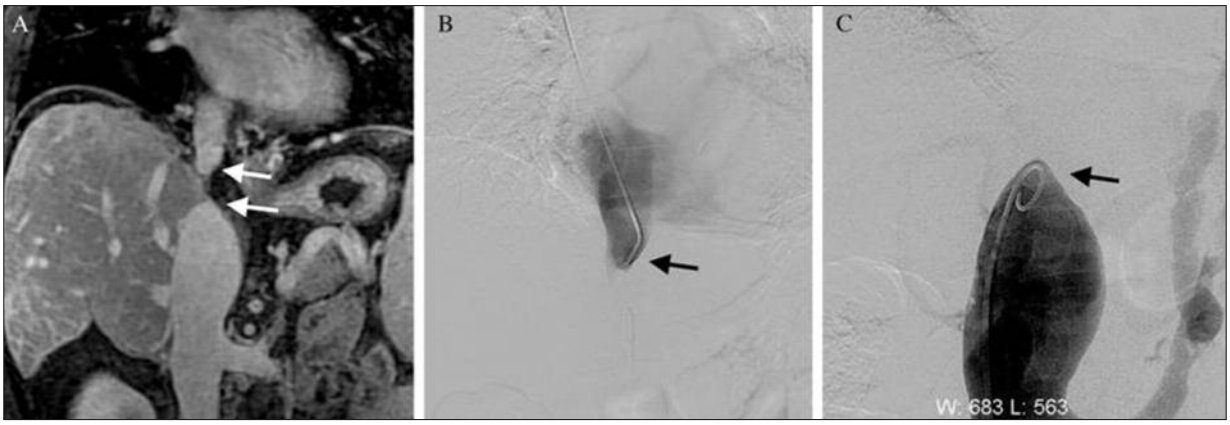

Figure 4. MRV and DSA images of an IVC obstruction with cone-shaped ends. ***A,*** MRV image showing an IVC obstruction with cone-shaped ends on both the proximal and distal sides (*arrows*). ***B,*** and ***C,*** DSA bidirectional images of a cone-shaped occluded end on the proximal ***(B)*** and distal ***(C)*** sides.

bined with collateral vessels. In contrast, MRV detected 36 cases with multiple collateral vessels and correctly detected all 3 dangerous communicating branches with expansion vessels that do not correspond to the azygos or hemiazygos veins.

There were 14 cases with occlusions combined with thrombosis at the distal end of the IVC. Of these, 2 cases were stenoses with membranous obstruction combined with thrombosis. One out of 2 cases was correctly detected by MRV, and 1 of 2 cases with old thromboses was also correctly detected by MRV. In all 14 patients, MRV clearly showed the range of thrombosis, spatial relationship between the wall of the IVC and the thrombi, and relationships among the hepatic orifice, accessory hepatic vein orifice and the thrombi.

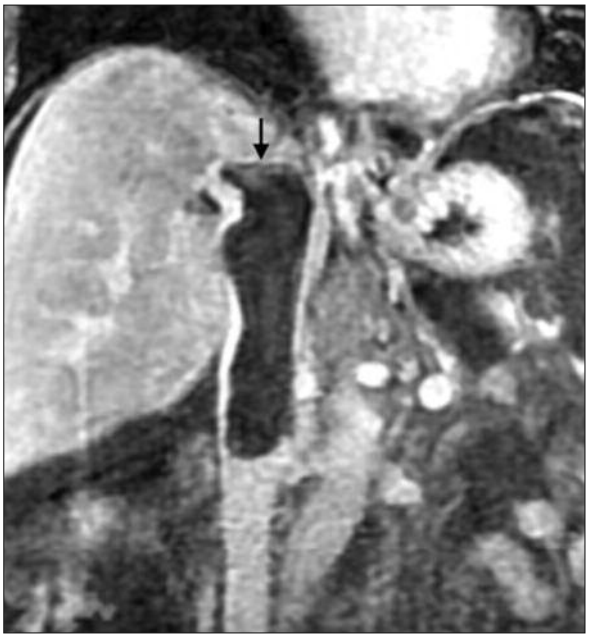

Figure 5. MRV image of an IVC occlusion case combined with thrombosis. The irregularly shaped thrombus is adjacent to the plateau-shaped distal side of the obstruction (*arrow*).

Discussion

Depending on their severity, IVC occlusion caused by BCS can be divided into partial and complete obstruction. Interventional treatment for patients presenting with partial obstruction consists of balloon dilation by femoral vein puncture. In patients with complete obstruction patients, treatment depends on the result of DSA two-directional imaging. Varied morphologies of

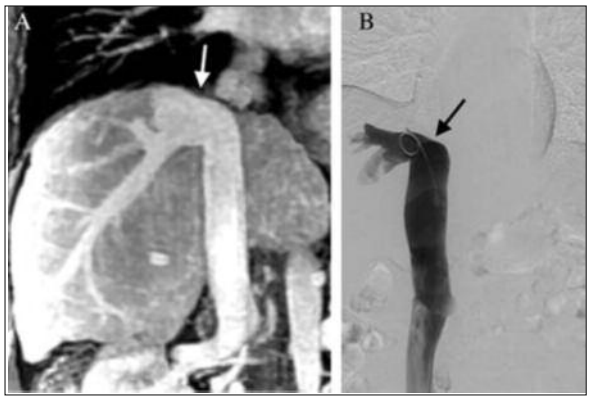

Figure 6. MRV and DSA images of a plateau-shaped obstructed IVC. ***(A)*** MRV image and ***(B),*** DSA image showing the distal side of the obstruction (*arrows*).

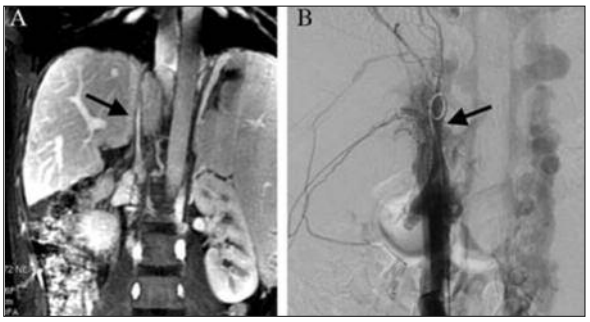

Figure 7. MRV and DSA images of an irregularly-shaped occluded distal end. ***A,*** MRV image of a tail-shaped occluded distal end (*arrow*). ***B,*** DSA image of an irregularly-shaped occluded distal end (*arrow*).

IVC occluded ends (cone, plateau-shaped, or irregularly-shaped), existence of collateral vessels, especially those that originate from the occluded side of IVC, and thrombosis formation inside the IVC make intervention difficult and lead to many complications[15,16]. MRV offers many advantages over DSA: the scans are non-invasive, provide high tissue resolution, and allow visualization of vascular flow void effect. Identifying the morphology of the occluded side of the IVC and assessing the existence of combined risk factors can assess preliminarily the difficulty of treatment and provide the foundation for choosing the optimal treatment regimen, therefore, reducing and even preventing complications during interventional treatment.

To date, no reports on MRV findings of partial IVC occlusion with membranous obstruction have been published. In the coronal position, high speed jet of blood through stenotic vessels with membranous obstruction is visualized as a flow void signal in a thin stripe. This "jet sign" can be seen in the contrast-enhanced vessels and is a more intuitive indication of IVC membrane occlusion than image analysis using DSA. In the literature, this stripe-like flow void signal has been erroneously reported as the signal caused by a membranous obstruction in the IVC. Usually the signal from a membranous obstruction in the IVC is horizontal or vertical, but not parallel to the wall of IVC. This may be related to the formation of the membranous obstruction. Identification of the actual cause will require further study. In our study, MRV correctly diagnosed 5 cases with membranous obstruction, and the jet sign was detected in all patients. However, in one case, where membranous obstruction was combined with thrombosis, the jet sign was not observed. The failure to observe the jet sign was probably due to a reduction in blood flow caused by blood clots, thus, preventing the contrast agent from forming a jet-like flow. Among the group of partially obstructed patients, there were 2 cases with segment stenosis that were misdiagnosed as complete obstructions. The misdiagnosis was possibly due to the relatively long range of stenosis leading to an extremely narrow lumen that could not be detected using MRV.

In patients with complete IVC obstructions, the choice of the direction of puncture is dependent on the morphology of the proximal or distal end of the occlusion to the heart.[1] MRV can display both sides of the occlusion in a single scan. When the occlusion is cone-shaped, the tip of the occlusion

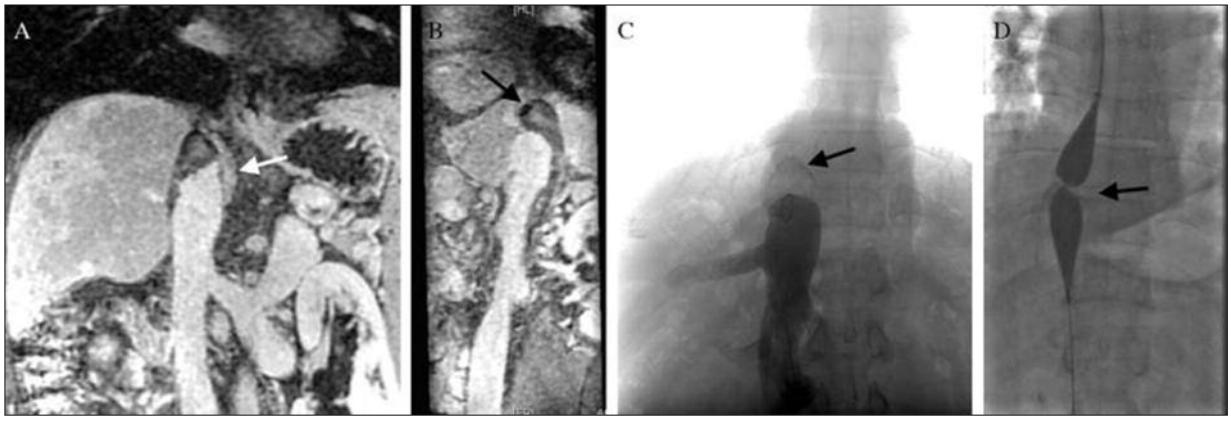

Figure 8. MRV and DSA images of calcification at the occluded end of the IVC. ***A,*** and ***B,*** MRV coronal ***(A)*** and sagittal ***(B)*** scans show that the distal end of the obstruction is not completely enveloped by calcification (*arrows*). ***C,*** and ***D,*** DSA images before ***(C)*** and after ***(D)*** needle penetration cannot display the three-dimensional relationship of the calcification (*arrows*) and the distal end of the obstruction. In this case, the balloon could not expand the calcified vessel segment.

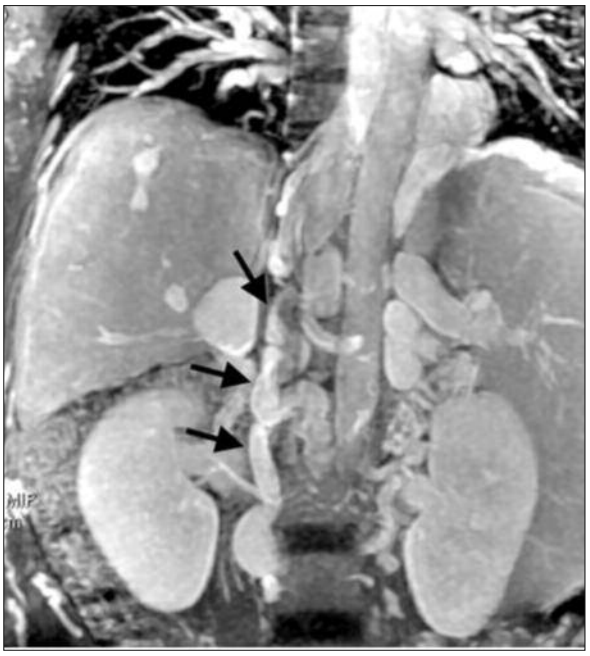

Figure 9. MRV image of an IVC obstruction presenting with distorted paraspinal vasculature. The distorted vasculature is indicated with a*rrows*.

has potential weak points. Specifically, in partial interventional treatment, exploration using guide wire with a hard head can find the weak points within. These weak points can be observed directly using MRV, which greatly aids interventional treatment. Additionally, in cases of membranous obstruction, if the pressure on the distal end is high, the membrane will bulge toward the low pressure side (proximal end), thus distorting into a fornix. This fornix is indicative of thin membrane where penetration is easy to achieve. The formation of plateau-shaped membranous obstruction indicates that the membrane is relatively tough and has no weak point. Thus, the area that can receive the puncture is larger. During the puncture procedure, the needle can easily slide into an angle directed between the diaphragm and the side wall of IVC. If the puncture is performed at that angle, the needle is prone to piercing the IVC which results in many complications. Thus, the observation of the platform-shaped obstruction defines the choice of interventional treatment to be taken. Irregularly-shaped obstruction is more common in cases combined with thrombosis, or other complex-type obstructions.

Some of the IVC obstruction patients presented with one or several abnormally-running collateral vessels originating from the obstructed side of the IVC, or a locally distorted and expanded vasculature (Figure 8). When performing interventional treatment, the guide wire can mistakenly enter the dangerous collateral vessels instead of the stenotic segment. Wire-mediated expansion of these collateral vessels may lead to sudden vessel rupture and hemorrhage. For this reason, these collateral vessels are termed dangerous collateral vessels. Dangerous communicating branches (DCB) are different from collateral vessels. We define the existing blood vessels with compensatory expansion as collateral circulation, such as azygos or hemiazygos veins. In contrast, we call vessels with abnormal expansion due to the obstruction that has not yet been named DCB. DCB include communicating branches among the obstructed hepatic veins and at obstructed end of the inferior vena cava. Therefore, the diagnosis of dangerous collateral vessels is critical to avoid the rupture and bleeding of the IVC during the intervention.

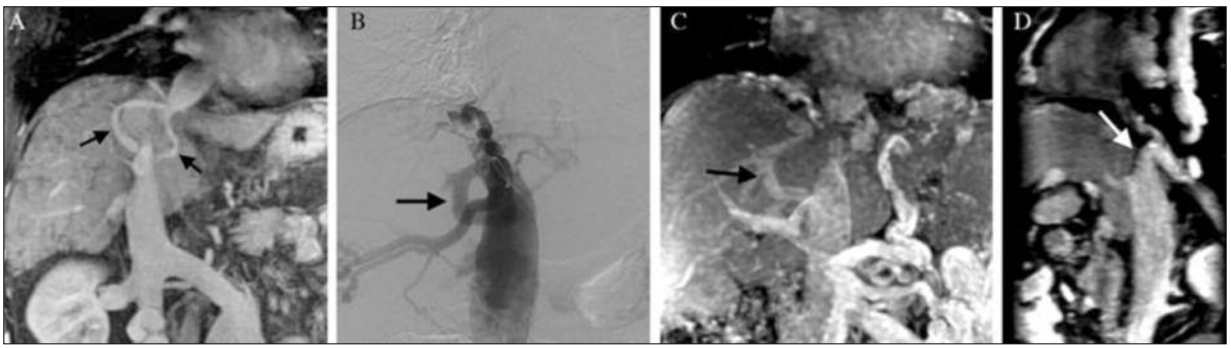

Figure 10. MRV and DSA images of IVC obstructions with dangerous collateral vessels. ***A,*** MRV image of a case with IVC obstruction with collateral vessels. The collateral vessels branching from the distal side of the obstruction are indicated with arrows. ***B,*** DSA image of a dangerous communicating branch (DCB) on the right side of the distal end of occlusion (*arrow*). ***C,*** and ***D,*** MRV images of DCBs on the right ***(C)*** and top ***(D)*** of the distal end of the occlusion (*arrows*).

In our study, we were able to observe collateral vessels in the distal end of the IVC using MRV. MRV can be used to observe targeted vessels in a multi-angle and multi-directional way and can accurately show the spatioanatomic location of collateral vessels, enabling the physician to judge whether the vessel targeted for puncture is a collateral one. In contrast, when using conventional 2D DSA imaging, it is hard to accurately judge the anatomy of the collateral vessels. Since MRV is non-invasive, it is of higher clinical value than conventional 2D DSA.

The optimal MRV scanning method for the diagnosis of IVC obstruction is thin layer scanning followed by scanning parallel to the vessels. In this study, we employed a 3D mode of breath-hold fast liver accelerated volume acquisition (LAVA) imaging and thin layer scanning at the entrance of the IVC to the second hepatic portal. Since 3.0T MRI has not been able to achieve true isotropy so far, we chose to perform a three-stage scan in the axis, coronal and sagittal positions. These scan parameters were shown in Table II. Through special K space filling technology, LAVA technology achieves fast, thin-layer volume scanning. LAVA is 25% faster and has greater resolution than the previous version of abdominal dynamic enhancement technology. LAVA can also cover a 25% larger range and it is superior for fat-suppression. The thin-layer volume scanning can continuously display the morphology of the vascular openings which can be observed at any angle after the images have been processed with the instrument software. Additionally, this technique can easily display microscopic anatomical details. Furthermore, thin-layer volume scanning can perform vessel MIP reconstruction while the lesions are being observed, which is significantly superior to thick layer scanning and generates a more accurate image of the occluded side of the IVC as compared with DSA imaging. The MRV images reconstructed from multiple planes better, compared with DSA, represent the three-dimensional structure of the IVC occlusion and of the adjacent tissue. As shown in Figure 8, irregular calcification can sometimes be observed in the distal end of IVC occlusion. In this case, conventional needle puncture was performed to penetrate the thick calcified areas and, then, the balloon was introduced. However, the balloon was not able to expand the occluded segment. The MRV image showed that the calcified area did not completely cover the end of the IVC. Such information enabled us to bypass the calcification by adjusting the puncture angles, so that membrane penetration and subsequent vessel expansion were achieved. In terms of visualizing the collateral vessels adjacent to the occlusion and predicting the existence of DCB, MRV imaging enables the visualization of the 3D spatial relationship with the IVC and its collateral branches in a more comprehensive manner than DSA. This is especially evident when collateral branches open in front of or behind the distal end of IVC obstruction, where 2D DSA imaging cannot access to the collateral vessel opening due to the blockage of the IVC. In contrast, MRV imaging enables the visualization of the position of collateral branches, thus, providing valuable information to the evaluation of the risks of concomitant treatment (Figure 10). The application of MRV has substantially reduced the need for DSA imaging and the exposure of patients to radiation. During the course of our study, one liver transplantation patient was also included. Using MRV, we diagnosed the patient with IVC stenosis and proved it through the use of DSA. Therefore, MRV imaging could also be applied to liver transplantation patients in order to observe the orifices of the vessels.

In this study, 14 cases with IVC obstruction were combined with thrombosis. MRV correctly diagnosed the morphology of the thrombus and its spatial relationship with the vessel wall and the hepatic vein. Fresh thrombi may cause acute thrombosis. During interventional treatment, special attention should be paid to avoid acute thrombosis. Due to the small sample size in our study, the proper and comprehensive assessment of thrombosis will need to be studied further.

Table II. Scan parameters for MRV diagnosis of IVC obstruction.

Parameter	Value	Reconstructed value
Axis position thickness	4.4 mm	2.2 mm
Coronal position thickness	3.6 mm	1.8 mm
Sagittal position thickness	3.2 mm	1.6 mm

Conclusions

In summary, MRV imaging is a valuable technique for diagnosing IVC obstruction. MRV imaging enables to observe the morphology of obstruction in the IVC, and provides critical information for interventional treatment of IVC occlusion. This information cannot be generated with two DSA unidirectional angiographies. Additionally, MRV imaging reduces radiation exposure during the intervention procedure. It can be utilized as a quick diagnostic tool and a substitute for DSA when planning optimal treatments.

Funding

This study was supported by grants from the Clinical Medical Science and Technology Project of Jiangsu Province (BL2012044) and the Science and Technology Project of Xuzhou City (XZZD1154).

Conflict of Interest

The Authors declare that there are no conflicts of interest.

References

1) Eapen CE, Velissaris D, Heydtmann M, Gunson B, Olliff S, Elias E. Favourable medium term outcome following hepatic vein recanalisation and/or transjugular intrahepatic portosystemic shunt for Budd Chiari syndrome. Gut 2006; 55: 878-884.
2) Surendrababu NR, Keshava SN, Eapen CE, Zachariah UG. Transjugular intrahepatic portocaval shunt placed through the strut of an inferior vena cava stent in a patient with Budd-Chiari syndrome: a technical modification. Br J Radiol 2010; 83: e22-24.
3) Gao Y, Chen S, Yu C. Applicability of different endovascular methods for treatment of refractory Budd-Chiari syndrome. Cell Biochem Biophys 2011; 61: 453-460.
4) Carnevale FC, Santos AC, Tannuri U, Cerri GG. Hepatic veins and inferior vena cava thrombosis in a child treated by transjugular intrahepatic portosystemic shunt. Cardiovasc Intervent Radiol 2010; 33: 627-630.
5) Hasija RP, Nagral A, Marar S, Bavdekar AR. Transjugular intrahepatic portosystemic shunt (TIPSS) for Budd Chiari syndrome. Indian Pediatr 2010; 47: 527-528.
6) Desai SK, Al-Bawardy BF, Leggett C, Gorospe EC. Recurrent bilateral pleural effusions without ascites as an initial presentation of Budd-Chiari syndrome. Ann Gastroenterol 2014; 27: 74.
7) Seijo S, Plessier A, Hoekstra J, Dell'era A, Mandair D, Rifai K, Trebicka J, Morard I, Lasser L, Abraldes JG, Darwish Murad S, Heller J, Hadengue A, Primignani M, Elias E, Janssen HL, Valla DC, Garcia-Pagan JC; European Network for Vascular Disorders of the Liver. Good long-term outcome of Budd-Chiari syndrome with a step-wise management. Hepatology 2013; 57: 1962-1968.
8) Flor N, Zuin M, Brovelli F, Maggioni M, Tentori A, Sardanelli F, Cornalba GP. Regenerative nodules in patients with chronic Budd-Chiari syndrome: a longitudinal study using multiphase contrast-enhanced multidetector CT. Eur J Radiol 2010; 73: 588-593.
9) Xu K, Feng B, Zhong H, Zhang X, Su H, Li H, Zhao Z, Zhang H. Clinical application of interventional techniques in the treatment of Budd-Chiari syndrome. Chin Med J (Engl) 2003; 116: 609-615.
10) Bogin V, Marcos A, Shaw-Stiffel T. Budd-Chiari syndrome: in evolution. Eur J Gastroenterol Hepatol 2005; 17: 33-35.
11) Wang L, Lu JP, Wang F, Liu Q, Wang J. Diagnosis of Budd-Chiari syndrome: three-dimensional dynamic contrast enhanced magnetic resonance angiography. Abdom Imaging 2011; 36: 399-406.
12) Yang C, Xu K, Zheng J, Ma P, Hu C, Li S, Rong Y, Lu X, Zhang Q, Zu M, Hua R, Zhang L. Hepatocellular carcinoma in Budd-Chiari syndrome: enhancement patterns at dynamic gadolinium-enhanced T1-weighted MR imaging. Cell Biochem Biophys 2014; 70: 661-666.
13) Tang W, Zhang XM, Yang L, Mitchell DG, Zeng NL, Zhai ZH. Hepatic caudate vein in Budd-Chiari syndrome: depiction by using magnetic resonance imaging. Eur J Radiol 2011; 77: 143-148.
14) Valla DC. Primary Budd-Chiari syndrome. J Hepatol 2009; 50: 195-203.
15) Beckett D, Olliff S. Interventional radiology in the management of Budd Chiari syndrome. Cardiovasc Intervent Radiol 2008; 31: 839-847.
16) Cura M, Haskal Z, Lopera J. Diagnostic and interventional radiology for Budd-Chiari syndrome. Radiographics 2009; 29: 669-681.